J. PATRICK REILLY

ELECTRICAL MODELS FOR NEURAL EXCITATION STUDIES

Natural bioelectric processes are responsible for nerve and muscle function and are affected by externally applied electric currents that may be intentionally introduced through medical devices or unintentionally introduced through accidental electric shock. Neuroelectric stimulation has been studied at APL by using a computer simulation that models the interaction of electric currents with nerve cells. The model successfully represents a variety of experimental observations. This article describes the physiological basis of the model and illustrates its properties.

INTRODUCTION

Nerve and muscle function depends on natural bioelectric phenomena. The mechanisms responsible for normal function will also respond to externally applied currents. With appropriate controls, electrical currents can provide medical assistance and diagnostic benefits such as muscle control, pain relief, sensory prosthesis, and the diagnosis of nerve and muscle function. However, in chance encounters with electric currents (electric shock), the result can be pain, hazardous muscle reactions, heart disturbances, and even death.

Whether our interest in electrical stimulation concerns intentional or accidental exposures, understanding the responsible mechanisms is important to help guide experiments and to study effects that are not readily amenable to an experimental approach. Research at APL has focused on the study of electrical excitation models based on principles of excitable membranes and has provided an explanatory framework for a variety of electrical stimulation applications.

A previous article[1] reported on experimentally determined factors that account for sensory potency of electrocutaneous stimulation. This article focuses on theoretical models for understanding how the spatial and temporal aspects of the stimulus affect neural excitation sensitivity.

ELECTRICAL FUNCTION OF NERVOUS TISSUE

Figure 1 illustrates several functional components of sensory and motor (muscle) neurons. The neurons are myelinated, i.e., covered with a fatty layer of insulation called myelin, and have exposed nodes of Ranvier. Other neurons are unmyelinated. Physiologists commonly classify myelinated and unmyelinated fibers as A- and C-fibers, respectively. The conducting portion of the neuron is a long, hollow structure known as the axon. The axon plus myelin wrapping is frequently referred to as a nerve fiber. The arrows in Fig. 1 indicate the direction of information flow. For the motor neuron in Fig. 1a, nerve impulses called action potentials (APs) propagate from synapses in the spinal column to the terminus at the muscle. For the sensory neuron in Fig. 1b, APs originate from one of a variety of specialized receptors (a Pacinian corpuscle is illustrated) and proceed to a synapse in the spinal column. Communication across the synapses is accomplished through chemical substances known as neurotransmitters.

An understanding of the electrical basis for nerve and muscle function is necessary for the development of predictive models for electrical excitation. This article first examines some basic electrical properties of biological cells and then examines the function of a special class of those cells having electrically excitable membranes.

Cellular Membranes

Cells are the basic building blocks of both plant and animal life. The functional boundary of the cell is a thin (about 8-nm) biomolecular lipid and protein layer. One role of the membrane is to regulate chemical exchanges between the area inside the cell (the plasm) and the area outside the cell (the interstitial fluid). The electrochemical forces across the membrane are significantly involved in the regulation.

The plasm and interstitial fluids are composed largely of water containing ions of different species. The difference in the concentration of ions causes electrochemical forces across the cell membrane. The membrane, which is semipermeable, is basically a dielectric insulator that allows some ionic interchange. Figure 2 represents a membrane as a barrier with pores that permit the passage of ions. The individual pores may be very selective of the ionic species they allow to pass. Typical concentrations inside and outside the cell are shown in Table 1 for Na^+, K^+, and Cl^- ions. Although other species are also present, confining our attention to these ions is sufficient for our purposes.

The concentrations indicated in Table 1 are markedly different inside and outside the cell. The differences in concentration result in two forces that tend to drive ions across the membrane: a concentration gradient and a voltage gradient. To understand these forces, first consider an environment where only one ionic species, substance S, is present.

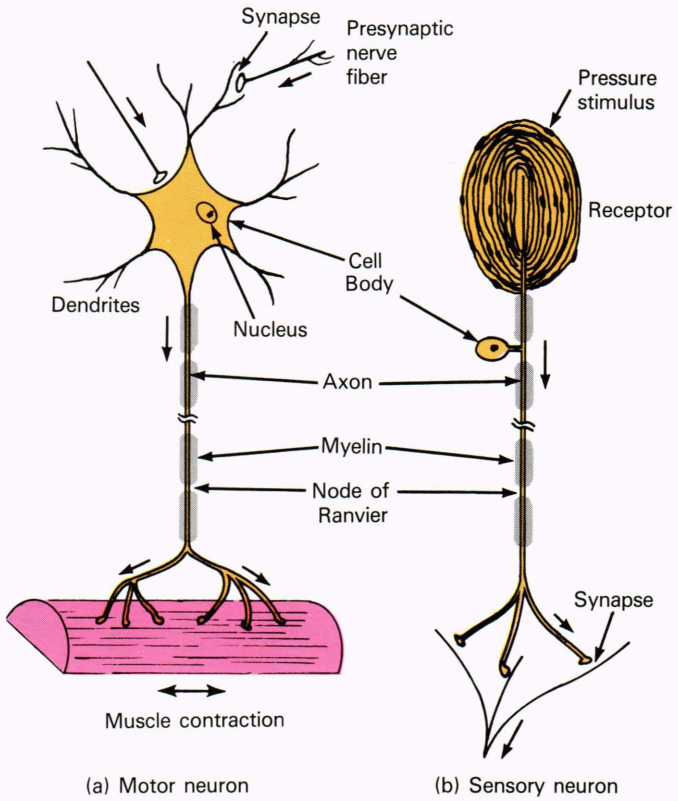

Figure 1—Functional components of (a) motor and (b) sensory neurons. Arrows indicate the direction of information flow. Signals are propagated across synapses via chemical neurotransmitters and elsewhere by membrane depolarization. Synapses are inside the spinal column. The sizes of the components are drawn on a distorted scale to emphasize various features.

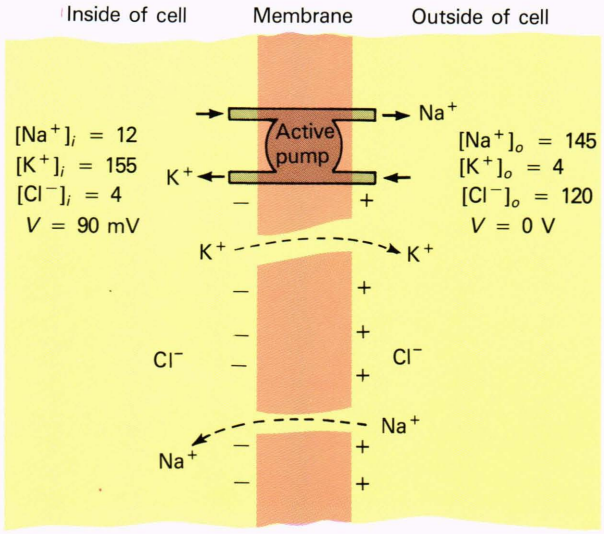

Figure 2—Schematic of a typical cell membrane. The pores allow the passage of ions. Numerical values indicate approximate steady-state concentrations (μmol/cm^3) for typical mammalian muscle cells. An active metabolic pump drives Na^+ out of the cell and K^+ into the cell. The transmembrane potential difference is about −90 mV; the inside is negative relative to the outside.

Table 1—Typical cellular ionic concentrations.

Ion Species	*Concentration (μM) Inside*	*Outside*	*Nernst Potential (mV)*
A. Mammalian muscle cells			
Na^+	12	145	66
K^+	155	4	−97
Cl^-	4	120	−90
	Resting potential		−90
B. Squid axon			
Na^+	50	460	59
K^+	400	10	−98
Cl^-	40 to 100	540	−45 to −69
	Resting potential		−60

Note: Adapted from Ruch and Patton[2] and Katz.[3]

In a solution where the concentration varies from one region to another, a net flux will occur from the region of higher concentration to the region of lower concentration. The concentration potential energy difference, W_c, is the work required to move a mole of S against the gradient. This quantity is proportional to the logarithm of the concentration difference in accordance with

$$W_c = RT\,(\ln [S]_i - \ln [S]_o) = RT \ln \frac{[S]_i}{[S]_o}\,, \quad (1)$$

where $[S]_i$ and $[S]_o$ represent the concentrations of S inside and outside the cell, respectively, R is the universal gas constant, and T is the absolute temperature. The product RT has units of energy per mole.

If S is ionized, an electrical potential difference will occur between the two regions of differing concentration. The electrical potential energy, W_e, is given by

$$W_e = Z F V_m , \quad (2)$$

where Z is the valence of S, F is the Faraday constant (number of coulombs per mole of charge), and V_m is the potential difference across the membrane.

The total electrochemical potential difference is the sum of the concentration and electrical potentials:

$$\Delta W = W_c + W_e . \quad (3)$$

Substituting the quantities from Eqs. 1 and 2 results in

$$\Delta W = RT \ln \frac{[S]_i}{[S]_o} + Z F V_m . \quad (4)$$

When $\Delta W = 0$, S is at equilibrium across the membrane (i.e., no net force occurs in either direction), and the net flux across the membrane is zero. Under conditions of equilibrium, the membrane will attain the potential

$$V_m = \frac{RT}{FZ} \ln \frac{[S]_o}{[S]_i} . \quad (5)$$

Equation 5 is known as the Nernst equation. It is a statement of the membrane potential for an ionic substance in electrochemical equilibrium. Using the values $R = 8.31$ J/mol K, $T = 310$ K (37°C), $F = 96{,}500$ C/mol, and $Z = +1$ (for a monovalent cation), converting to the base 10 logarithm, and expressing V_m in millivolts, we obtain

$$V_m = 61 \log \frac{[S]_o}{[S]_i} . \quad (6)$$

For a system with more than one ionic species, the equilibrium voltage will depend on the concentration and relative permeability to the individual ions. For a system consisting of K^+ and Na^+, for example, the expression is

$$V_m = 61 \log \frac{P_K[K^+]_o + P_{Na}[Na^+]_o}{P_K[K^+]_i + P_{Na}[Na^+]_i} , \quad (7)$$

where P_K and P_{Na} are the permeabilities (cm/s) to K^+ and Na^+, respectively. An alternate expression for Eq. 7 uses the ratio $q = P_{Na}/P_K$ to obtain

$$V_m = 61 \log \frac{[K^+]_o + q\,[Na^+]_o}{[K^+]_i + q\,[Na^+]_i} . \quad (8)$$

One can get a feel for the changes in V_m during excitation by considering the simplified circuit diagram in Fig. 3. The membrane permeability is represented by conductances g_{Na} and g_K, and the electrochemical gradients are represented as potential sources E_{Na} and E_K. For an excitable membrane in the resting state, $g_{Na} \ll g_K$, and the membrane potential approaches the Nernst potential for K^+, as indicated by Eq. 8. In the excited state, $g_{Na} > g_K$, and the switches in Fig. 3 would be connected in their alternate positions, forcing the membrane to move toward the Nernst potential for Na^+.

Consider now the individual Nernst potentials for the ionic species listed in the right-hand column of Table 1. The equilibrium potential for Na^+ (66 mV) is far removed from the membrane potential (−90 mV), K^+ is slightly out of equilibrium, and Cl^- is essentially in equilibrium. The magnitudes and signs of the potentials show a strong electrochemical force tending to drive Na^+ into the cell and a relatively weaker force tending to drive K^+ out of the cell. Given that the membrane is at least somewhat permeable to the ions discussed here, these forces ought eventually to bring the species into equilibrium. Clearly, another force is working to maintain the system in disequilibrium. The responsible force is the so-called sodium pump, an active system that pumps Na^+ out of the cell and K^+ into the cell. The energy for the pump is derived from the cell's metabolism. A dead cell would eventually reach equilibrium potential.

The electrical forces on the membrane are quite large. Considering the membrane potential ($\approx 10^{-1}$ V) and thickness ($\approx 10^{-8}$ m), the electric field developed across the membrane is about 10^7 V/m. Conductivity properties of the excitable membrane are intimately tied to the

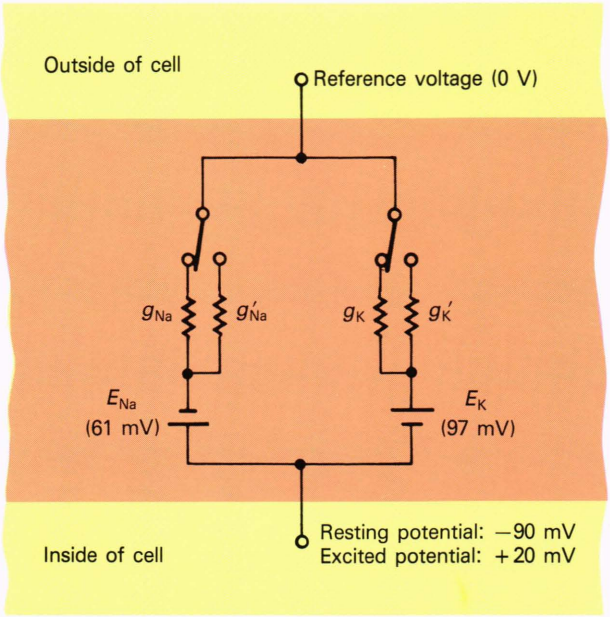

Figure 3—Circuit diagram representing membrane conductance for Na^+ and K^+ ions. In the resting condition, the inside of the cell is at a potential of −90 mV. In the excited state, the inside of the cell is at a potential of 20 mV.

membrane field; disturbances from the resting condition can lead to profound changes in the membrane's electrical properties. These changes ultimately initiate and sustain the functional responses of nerve and muscle.

The Excitable Membrane

Nerve and muscle cells possess membranes that are excitable to the extent that an adequate disturbance of the cell's resting potential can trigger a sudden change in the membrane conductance. The resulting membrane voltage change will affect adjacent portions of the membrane and, in a nerve, will propagate as a nerve impulse. The response of the excited membrane is known as an action potential.

To illustrate the properties of excitability and propagation, consider the experiment illustrated in Fig. 4 in which a small stimulating electrode (SE) is near a nerve fiber and two small recording microelectrodes (RE) pierce the membrane; the return electrodes are assumed to be immersed in the conducting medium some distance away. The stimulating electrode is connected to a current source. In Fig. 4, the arrows represent the distribution of current flow if the SE is a cathode, showing cationic flow toward the cathode. The voltage disturbance caused by the stimulating electrode will tend to decrease the membrane potential (depolarization) near the cathode and increase the potential (hyperpolarization) elsewhere along the axon.

Figure 5 illustrates the response of the membrane to the rectangular current pulses shown in the upper part of the figure. Six possible current magnitudes, labeled a through f, are shown. Pulses a through c apply if the SE is an anode; pulses d through f apply if the SE is a cathode. The membrane response is shown as measured by RE1 and RE2, where 0 mV represents the resting potential. Responses a through c are in the direction of hyperpolarization, and responses d through f are in the direction of depolarization. Responses a through d exhibit the characteristic of a linear network consisting of a parallel combination of a resistor and a capacitor. As a critical level of depolarization is approached (approximately 20 mV in Fig. 5), nonlinear behavior is seen. Response e is slightly below the excitation threshold, and response f illustrates a fully developed AP. The signal at RE2 is a delayed version of the AP, demonstrating conduction along the axon. The membrane response is often referred to as "all or nothing" because the peak AP response is not normally graded; i.e., the membrane is either excited or it is not.

To develop a quantitative model of excitation of the neuron by externally applied currents, nonlinear membrane models and transmission line theory must be used. Let us begin with an understanding of membrane events associated with the production of an AP.

In Fig. 2, the membrane can be treated as a lossy capacitor. The membrane itself acts as the dielectric, and the ions on either side of the membrane act as the conductive plates of the capacitor. The nature of the leakage channels in the dielectric distinguishes the excitable membrane from the ordinary cellular membrane.

The Hodgkin–Huxley Membrane. A detailed description of the electrical properties of the excitable membrane was developed by Hodgkin and Huxley.[4] With a series of ingenious experiments that eventually led to a Nobel Prize, they provided the first detailed description of the electrical properties of the excitable membranes of unmyelinated nerve cells. This work was later extended by Frankenhaeuser and Huxley[5] to describe the myelinated nerve membrane. For brevity, we shall refer to the Hodgkin–Huxley and Frankenhaeuser–Huxley work as HH and FH equations, respectively. The HH and FH equations are largely empirical.

Figure 6 illustrates schematically the HH membrane. The electrical model consists of membrane capacitance, nonlinear conductances for Na^+ and K^+, and a linear leakage element. For a parallel combination of capacitance and conductance, the current through the membrane is related to the capacitive and leakage currents by

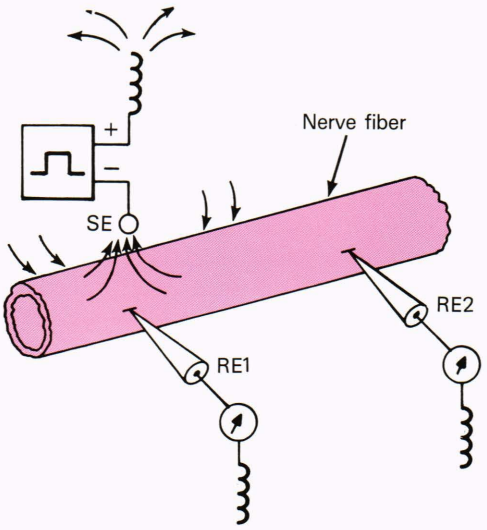

Figure 4—Nerve excitation and measurement arrangement. Excitation is initiated near the cathode of the stimulating electrode.

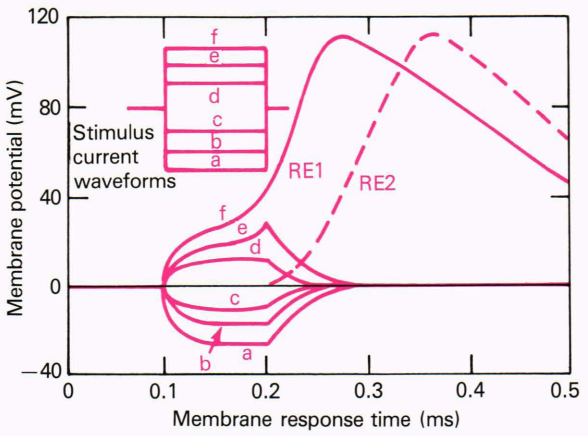

Figure 5—Excitation of a nerve fiber by an applied current, as in Fig. 4.

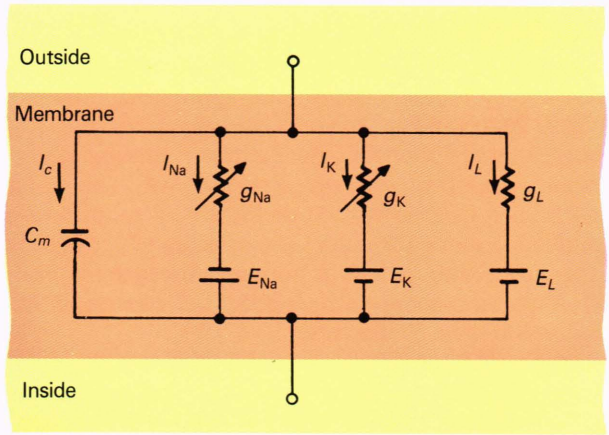

Figure 6—Hodgkin-Huxley membrane model.

$$J_m = c_m \frac{dV}{dt} + (J_{Na} + J_K + J_L) , \quad (9)$$

where J_m is the membrane current density; c_m is the membrane capacity (capacitance per unit area); V is the membrane voltage; and J_{Na}, J_K, and J_L are the ionic current densities. The ionic terms are expressed by

$$J_{Na} = g_{Na} (V - V_{Na}) , \quad (10)$$

$$J_K = g_K (V - V_K) , \quad (11)$$

and

$$J_L = g_L (V - V_L) , \quad (12)$$

where g_{Na}, g_K, and g_L are the ionic conductances; and V_{Na}, V_K, and V_L are the ionic Nernst potentials. The g_L conductance is linear; the other two conductances are more complex nonlinear functions of the form

$$g_{Na} = \bar{g}_{Na} m^3 h \quad (13)$$

and

$$g_K = \bar{g}_K n^4 , \quad (14)$$

where $\bar{g}_{Na}$ and $\bar{g}_K$ represent the maximum conductance values; and n, m, and h are so-called activation and deactivation variables that modulate the maximum conductances. The n, m, and h variables are governed by first-order differential equations:

$$\frac{dn}{dt} = \alpha_n (1 - n) - \beta_n n , \quad (15)$$

$$\frac{dm}{dt} = \alpha_m (1 - m) - \beta_m m , \quad (16)$$

and

$$\frac{dh}{dt} = \alpha_h (1 - h) - \beta_h h . \quad (17)$$

The α and β terms in Eqs. 15 through 17 are functions of the membrane voltage; their functional relationships are described in Ref. 4. Solutions to Eqs. 15 through 17 can be obtained in the form

$$n(t) = n_\infty - (n_\infty - n_0) e^{-t/\tau_n} , \quad (18)$$

$$n_\infty = \frac{\alpha_n}{\alpha_n + \beta_n} , \quad (19)$$

and

$$\tau_n = \frac{1}{\alpha_n + \beta_n} , \quad (20)$$

where $n(0) = n_0$, and $n(t \rightarrow \infty) = n_\infty$. Expressions similar to Eqs. 18 through 20 are obtained for $m(t)$ and $h(t)$. The n, m, and h variables are constrained between 0 and 1 and can be regarded as the fraction of ion gates that are open at any one time. As indicated by Eqs. 13 and 14, these gates modulate the maximum conductances of Na^+ and K^+. The τ_n, τ_m, and τ_h variables determine the rate at which the gates can open and close. The asymptotic values of the n, m, and h variables and the associated time constants are all functions of membrane depolarization voltage, as illustrated in Fig. 7.[6]

Depolarization of the membrane is necessary for excitation. Figure 8 illustrates the membrane events accompanying excitation of the HH membrane. Figure 8a shows the AP voltage waveform along with the membrane conductance. Figure 8b shows membrane current; the positive axis refers to current influx. An initial surge of Na^+ influx serves to further depolarize the membrane; this influx is followed by K^+ efflux, which repolarizes the membrane.

The Frankenhaeuser-Huxley Membrane. The FH equations for the myelinated membrane use four ionic terms in contrast with the three used for the HH membrane. The FH ionic current densities are

$$J = J_{Na} + J_K + J_p + J_L . \quad (21)$$

The terms J_{Na}, J_K, and J_L have the same interpretation as they do with the HH membrane. The term J_p was described as a nonspecific ionic component that responds to the concentration gradient of Na^+. The question of whether J_p represents a second type of Na^+ channel or another ionic species was left unresolved by FH.

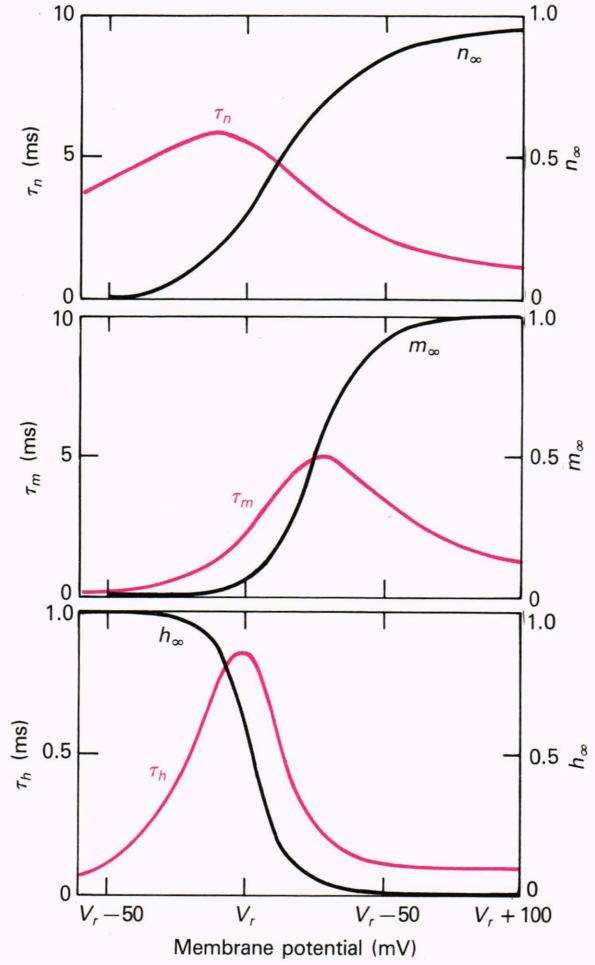

Figure 7—Relationship of m, n, and h constants to the membrane voltage. V_r represents the resting potential (adapted from Stein[6]).

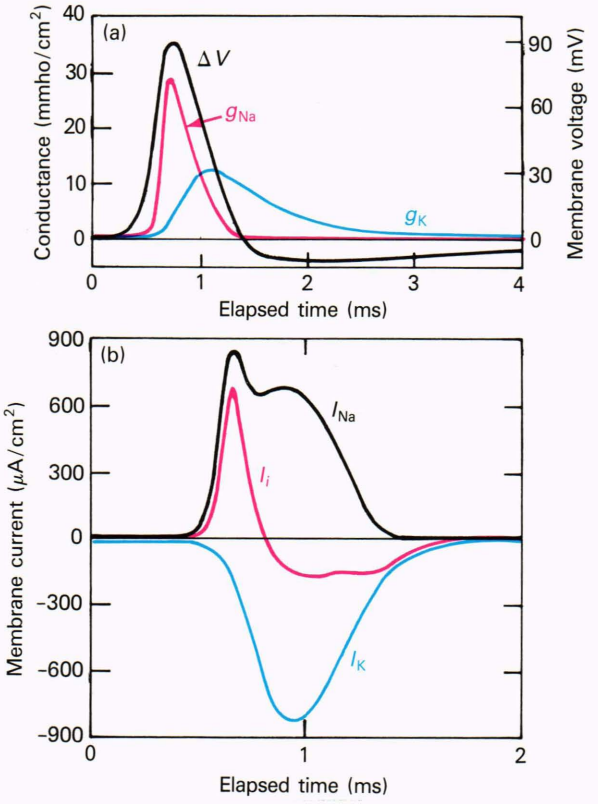

Figure 8—Membrane events during propagating action potential. The top figure (a) shows the membrane voltage change (ΔV) and the conductances g_{Na} and g_K. The bottom figure (b) shows the sodium current (I_{Na}), potassium current (I_K), and total ionic current (I_i). The positive axis indicates the ionic current influx (adapted from Hodgkin and Huxley[4]).

In the FH membrane, the individual ionic current densities have the expressions

$$J_{Na} = \bar{P}_{Na}\, h\, m^2 \left(\frac{EF^2}{RT}\right) \times \frac{[Na]_o - [Na]_i \exp(EF/RT)}{1 - \exp(EF/RT)}\,, \quad (22)$$

$$J_K = \bar{P}_K\, n^2 \left(\frac{EF^2}{RT}\right) \times \frac{[K]_o - [K]_i \exp(EF/RT)}{1 - \exp(EF/RT)}\,, \quad (23)$$

$$J_p = \bar{P}_p\, p^2 \left(\frac{EF^2}{RT}\right) \times \frac{[Na]_o - [Na]_i \exp(EF/RT)}{1 - \exp(EF/RT)}\,, \quad (24)$$

and

$$J_L = g_L\,(V - V_L)\,, \quad (25)$$

where $E = V - V_r$, V is the membrane potential, and V_r is the resting potential. The variables m, n, h, and p are defined by differential equations of a form identical to Eqs. 15 through 17. The α and β constants for the FH equations are given by

$$\alpha_m = 0.36\,(V - 22) \times \left[1 - \exp\left(\frac{-V + 22}{3}\right)\right]^{-1}, \quad (26)$$

$$\beta_m = 0.4\,(-V + 13) \times \left[1 - \exp\left(\frac{-V + 13)}{20}\right)\right]^{-1}, \quad (27)$$

$$\alpha_h = 0.1\ (-V - 10) \times \left[1 - \exp\left(\frac{V + 10}{6}\right)\right]^{-1}, \quad (28)$$

$$\beta_h = 4.5 \left[1 + \exp\left(\frac{-V + 45}{10}\right)\right]^{-1}, \quad (29)$$

$$\alpha_n = 0.02\ (V - 35) \times \left[1 - \exp\left(\frac{-V + 35}{10}\right)\right]^{-1}, \quad (30)$$

$$\beta_n = 0.05\ (-V + 10) \times \left[1 - \exp\left(\frac{V - 10}{10}\right)\right]^{-1}, \quad (31)$$

$$\alpha_p = 0.006\ (V - 40) \times \left[1 - \exp\left(\frac{-V + 40}{10}\right)\right]^{-1}, \quad (32)$$

$$\beta_p = 0.09\ (-\mathrm{V} - 25) \times \left[1 - \exp\left(\frac{V + 25}{20}\right)\right]^{-1}. \quad (33)$$

Specific constants for use in the FH equations are given in Table 2.

Differences between the FH and HH equations reflect the specific properties of the myelinated and unmyelinated membranes. The activation variables have different powers, and the FH equations have an additional ionic term. The ionic terms appear more complex in the FH membrane compared with those in the HH membrane. Despite the greater complexity of the FH equations, the electrical properties associated with the myelinated membrane's AP development are very similar to those associated with the HH membrane. One observed difference is a somewhat longer AP duration for the HH membrane. In addition, for a prolonged current stimulus, the HH equations produce multiple APs, whereas the FH membrane produces a single AP.[7]

Other differences are seen between myelinated (A-fiber) and unmyelinated (C-fiber) response when the overall excitatory behavior of the neuron is considered. Some of these differences include faster conduction rates and lower thresholds to external currents for A-fibers.[2] The A-fiber is an ideal one to model for electrical stimulation studies; because of its lower excitation threshold for external current stimulation, the A-fiber class will generally determine the limiting value for threshold currents.

Table 2—Constants for FH equations.

Constant	*Value*	*Description*
$\bar{P}_{Na}$	8×10^{-3} cm/s	Sodium permeability constant
$\bar{P}_K$	1.2×10^{-3} cm/s	Potassium permeability constant
$\bar{P}_p$	0.54×10^{-3} cm/s	Nonspecific permeability constant
g_L	30.3 mS/cm^2	Leakage conductivity
V_L	0.026 mV	Leakage equilibrium potential
$[Na]_o$	114.5 mM	External sodium concentration
$[Na]_i$	13.7 mM	Internal sodium concentration
$[K]_o$	2.5 mM	External potassium concentration
$[K]_i$	120 mM	Internal potassium concentration
F	96,514 C/g·mol	Faraday's constant
R	8.3144 J/K·mol	Universal gas constant
T	295.18 K	Absolute temperature

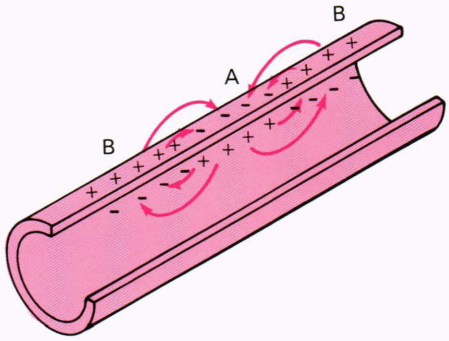

Figure 9—Spread of the depolarization wave front. Depolarization occurring in region A results in charge transfer from the adjacent regions.

Propagation of Nerve Impulses. The processes supporting AP propagation can be understood by referring to Fig. 9. Consider that point A on the axon is depolarized. The local point of depolarization causes ionic movement between adjacent points on the axon, thus propagating the region of depolarization. If depolarization were initiated from an external source on a resting membrane at point A, an AP would propagate in both directions away from the site of stimulation. Normally, however, an AP is initiated at the terminus of the axon and propagates in only one direction.

After the membrane has regained the resting potential, it cannot be reexcited until a recovery period has passed. This period is termed the refractory state of the membrane. Before full recovery, the membrane becomes partially refractory; i.e., it requires a stronger depolarizing force to become excited. The refractory property is prin-

cipally due to the prolonged decrease of the sodium deactivation variable, h, which effectively turns off the membrane's sodium conductance until the passage of a recovery period that extends beyond the repolarization process.

Refractory behavior in frog nerve is illustrated in Fig. 10.[3] The figure shows the membrane response to an external current stimulus. An initial stimulus, applied at $t = 0$, results in response a. Successive stimuli applied at various subsequent times lead to responses b through g. The absolute refractory period exists from the AP spike to somewhere within the negative after-potential. During this period, a second stimulus, no matter how strong, fails to produce a response. In a mammalian nerve at body temperature, the neuron is absolutely refractory for typically about 0.5 ms. Afterward, for a period of several milliseconds, the nerve is relatively refractory. During this period, an increased stimulus is needed to produce a response, and that response will initially be feeble, as shown by responses b through e. After several milliseconds, the neuron fully recovers from its less excitable state.

The refractory recovery period sets an upper limit on the number of APs per second that the membrane can support. With externally applied electrical stimuli, an AP rate cannot be produced beyond about 2000 per second. In natural conditions in the body, the repetition rate rarely exceeds 500 per second and is more typically in the range from 10 to 100 per second.[8]

The AP velocity depends on the rate at which electrical charge is transferred from the locus of excitation to the region of membrane ahead of the AP. The charge-transfer rate, in turn, depends on the membrane capacity and the longitudinal resistance of the axon. Depending on the assumptions made, theoretical arguments suggest that conduction velocity ought to vary as the square root of, or linearly with, fiber diameter.[9] Experimental evidence demonstrates that conduction velocity indeed increases with fiber diameter, and experimental data are frequently represented in terms of the ratio of conduction velocity to fiber diameter.[10]

The myelinated fiber is nature's means of obtaining fast conduction velocity without requiring unduly large fibers. The effective area requiring capacitive charging is mainly limited to the myelin-free nodes. Furthermore, the depolarization process is saltatory; i.e., it jumps from node to node. As a result, propagation can proceed at a much faster rate than would be the case with an unmyelinated fiber of the same diameter.

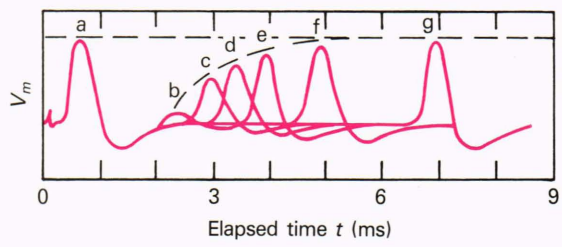

Figure 10—Illustration of the refractory period in frog nerve. The initial stimulus was applied at $t = 0$, resulting in response a. Subsequent stimuli were applied at various time delays, resulting in responses b through g (adapted from Katz[3]).

Table 3 lists some general characteristics of A- and C-fibers. The myelinated A-fibers are sometimes subdivided into diameter classes designated A_δ, A_β, and A_α. The A_δ fibers are typically related to cutaneous pain and temperature sensation, the A_β fibers are related to mechanoreception, and the A_α fibers are related to proprioception and contraction of striated muscle.[11] The distribution of A-fiber diameters is typically in the range from 2 to 20 μm.[12] Unmyelinated fibers typically range from 0.3 to 1.3 μm.

COMPUTATIONAL MODELS FOR ELECTRICAL STIMULATION

Electrical stimuli can vary enormously in sensory and neuromuscular potency. Variations in the stimulus waveform or in the electrode arrangement can result in vastly different stimulation thresholds. To understand the properties of a stimulus that determine its excitation potency, computational models may be used that connect features of the stimulus currents with properties of excitable tissue. Various computational models have been used to study the excitation properties of neural fibers. Excitation properties have been examined for a spatially isolated segment of membrane in which the current density crossing the membrane is the driving force. In these models, the membrane properties are modeled by the HH or FH equations that were discussed previously.

More complete representations include assumptions about mutual interactions among adjacent segments of the excitable membrane. One such model, developed by Cooley and Dodge,[13] uses a lumped equivalent circuit to represent an unmyelinated fiber, with stimulation by an intracellular electrode. In this model, membrane conductance is governed by the HH equations. Myelinated-fiber models studied by Fitzhugh[14] and Bostock[15] make explicit assumptions about the passive role of the myelin internode, in addition to the active FH conductances at the nodes. These models have also been configured to study excitation by injection of current at a single point on the axon.

A difficulty with the aforementioned nonlinear models is that they presume knowledge of the current waveform

Table 3—Characteristics of A- and C-fibers.

Characteristic	*Fiber Class*	
	A	*C*
Fiber diameter (μm)	1–22	0.3–1.3
Conduction velocity (m/s)	5–120	0.6–2.3
AP duration (ms)	0.4–0.5	2.0
Absolute refractory period (ms)	0.4–1.0	2.0
Velocity/diameter ratio (m/s·μm)	6	$\approx$1.7
Myelinated fiber	Yes	No

Note: Adapted from Ruch and Patton.[2]

and density crossing the membrane. In electrical stimulation problems, we may be able to calculate the current within the medium containing the neuron, but not necessarily the current crossing the membrane. The waveform of current crossing the membrane can differ substantially from that in the surrounding medium.[16] Furthermore, the force driving current into the membrane is the external field distribution along the axon, which cannot be described by the current density at a single point. These difficulties have been removed in the myelinated-fiber model of McNeal,[16] described in the following section.

Spatially Extended Nonlinear Models

Figure 11 illustrates the equivalent circuit representation of the myelinated nerve as formulated by McNeal.[16] The individual nodes are shown as circuit elements consisting of capacitance (C_m), resistance (R_m), and a potential source (E_r) that maintains the transmembrane resting potential. The current emanating from the stimulus electrode through the conducting medium causes external voltage disturbances ($V_{e,i}$) at the nearby nodes. These disturbances force current across the membrane.

In the McNeal[16] representation, the myelin internodes are treated as perfect insulators. This framework could be expanded to include passive myelin properties; however, such expansion would add significantly to the complexity of the model. The model is therefore a compromise between relatively simple single-node models and a more complete node-plus-myelin representation. Despite the compromise, the model is able to account for a variety of sensory and electrophysiological effects.

In Fig. 11, the current emanating from the nth node is the sum of capacitive and ionic currents and is related to internal axonal currents by

$$C_m \frac{dV_n}{dt} + I_{i,n} = G_a \left(V_{i,n+1} - 2\,V_{i,n} + V_{i,n+1}\right) , \tag{34}$$

where C_m is the membrane capacitance of the node, V_n is the transmembrane potential difference at the nth node, $I_{i,n}$ is the internal ionic current flowing in the nth node, and $V_{i,n}$ is the internal voltage at the nth node. In this expression, V_n is taken relative to the resting potential such that the resting potential is obtained at $V_n = 0$, and positive V_n applies to membrane depolarization.

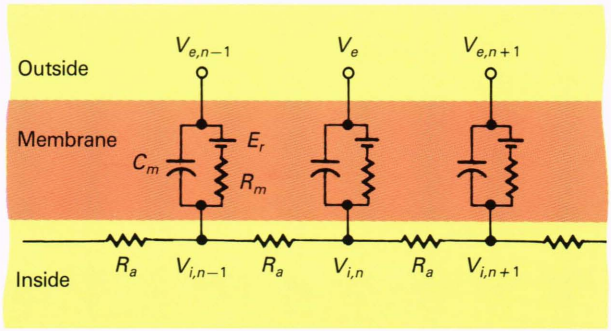

Figure 11—Equivalent circuit model for myelinated nerve fiber. Membrane conductance is described by the Frankenhaeuser-Huxley nonlinear differential equations (after McNeal[16]).

Further relationships are given by

$$G_a = \pi\, d^2/(4\,\rho_i\, L) , \tag{35}$$

$$G_m = g_m\, \pi\, d\, W , \tag{36}$$

and

$$C_m = c_m\, \pi\, d\, W , \tag{37}$$

where d is the axon diameter at the node, ρ_i is the resistivity of the axoplasm, L is the internodal gap, g_m is the subthreshold membrane conductance per unit area, c_m is the membrane capacitance per unit area, and W is the nodal gap width.

In Eq. 34, V_n is the voltage difference across the membrane,

$$V_n = V_{i,n} - V_{e,n} , \tag{38}$$

where $V_{i,n}$ and $V_{e,n}$ are the internal and external nodal voltages, respectively, with reference to a distant point within the conducting medium outside the axon. Substituting Eq. 38 into Eq. 34 results in

$$\frac{dV_n}{dt} = \frac{1}{C_m}\left[G_a \left(V_{n-1} - 2V_n + V_{n+1} + V_{e,n} - 2V_{e,n} + V_{e,n+1}\right) - I_{i,n}\right] . \tag{39}$$

In this equation, the $V_{e,n}$ values are specified from assumptions about the stimulus current distribution, and the V_n values are unknowns for which solutions must be found. The ionic current term can be expressed for either a linear or a nonlinear membrane:

$$I_{i,n} = G_m\, V_n \text{ (linear)} \tag{40a}$$

or

$$I_{i,n} = \pi\, d\, W \left(J_{\mathrm{Na}} + J_{\mathrm{K}} + J_L + J_p\right) \text{ (nonlinear)} . \tag{40b}$$

Equation 40a is a simple statement of Ohm's law for a linear conductor. Equation 40b applies to the nonlinear

ionic current expressions for the FH membrane given by Eqs. 22 through 25.

The most accurate representation would treat all the nodes in the model as nonlinear. However, such treatment can result in excessive computing time, which can be reduced by limiting the number of nonlinear nodes. In McNeal's original work,[16] he studied an 11-node array with one central node as nonlinear and all the others as linear. In his study, excitation current was introduced via an electrode nearby the central nonlinear node. He defined excitation as occurring when the nonlinear node reached a peak depolarization value of 80 mV. For the range of stimuli studied by McNeal, this arrangement was entirely satisfactory. However, for a more general range of stimulus parameters, some modifications are required.

The model described in this article is an extension of the one published by McNeal, with modifications to include FH nonlinearities at each of several adjacent nodes. Additional extensions include a test for excitation based on AP propagation, the ability to model arbitrary stimulus waveforms, the representation of stimulation at the neuron terminus, and the representation of stimulation by uniform electric fields. (The use of a single depolarization voltage is not always an adequate indicator of excitation when brief oscillatory stimuli are used. In that case, a threshold test based on propagation is needed.[17]) We shall refer to this modified representation of McNeal's model as the spatially extended nonlinear nodal (SENN) model. Unless otherwise noted, SENN model parameters used to obtain the data in this article are those given in Table 4. The listed parameters are those used originally by McNeal.[16] The SENN model was written in Fortran IV. The system of differential equations representing transmembrane currents was solved by using fourth-order Runge–Kutta iteration with initialization by the Gill technique. The time steps were typically 4 or 5% of the stimulus phase duration (or of its exponential time constant), but they were never greater than 2 μs.

To exercise the model, the spatial distribution of voltage along the axon as a result of the stimulating current must be specified. One voltage distribution used in this article is based on isotropic current propagation from a point electrode placed in a uniform medium. The indifferent electrode is taken to be in the conducting medium, far from the axon. Thus, the voltage at a radial distance, r, from the electrode is given by

Table 4—Example parameters for SENN model.

Parameter	*Value*
Fiber diameter, D	20 μm
Axon diameter, d	0.7 D
Nodal gap, G	2.5 μm
Axoplasmic resistivity, ρ_i	110 Ω·cm
External medium resistivity, ρ_e	300 Ω·cm
Membrane capacity, c_m	2 μF/cm^2
Membrane conductivity, g_m	30.4 mS/cm^2
Internodal distance, L	100 D

$$V(r) = \rho I/(4 \pi r) , \quad (41)$$

where ρ is the resistivity of the medium. In the general case, I and V are functions of time that follow the stimulus waveshape.

Another voltage distribution used in this article applies to stimulation by monophasic currents having a spatially uniform current density, thereby resulting in a uniform electric field. The electric field is related to current density by

$$E = \rho J , \quad (42)$$

where E is the electric field and J is the current density. In Fig. 11, the nodal voltages are given by

$$V_{e,n} = V_{e,1} + E L n , \quad (43)$$

where $V_{e,1}$ is a reference voltage at the terminal node, L is the internodal space, and n is the node number. In Eq. 43, it is assumed that the first node of the array is oriented toward the cathode of the current source.

Excitability Properties with Monophasic Stimulation

The membrane response of the SENN model to a rectangular current stimulus is illustrated in Fig. 12. The example is for a small cathodal electrode that is 2 mm radially distant from a 20-μm fiber and directly above a central node. The transmembrane voltage, ΔV, is scaled relative to the resting potential. Curves a–c show the response at the node nearest the stimulating electrode. Responses to three different cathodal pulse magnitudes, all of the same duration (100 μs), are depicted. Response a is for a pulse at 80% of the threshold current. Stimulus pulse b is at threshold, and pulse c is 20% above threshold. The threshold stimulus pulse in this example has an amplitude (I_T) of 0.68 mA.

Figure 13 illustrates threshold charge and current from the SENN model evaluated for anodal and cathodal rectangular stimuli with pulse durations of 1, 5, 10, 50, 100, 200, 500, 1000, 2000, and 10,000 μs. The plotted thresholds are known as strength/duration (S/D) curves. The vertical separation between the anodal and cathodal curves reflects the polarity selectivity ratio (P), which is the ratio of absolute thresholds for anodal/cathodal stimuli. The selectivity ratio is nearly constant, ranging from 4.2 at a pulse duration of 1 μs to 5.6 at a pulse duration of 10 ms. This range of P is consistent with in-vivo stimulation of nerve axons, although smaller ratios are observed with electrocutaneous sensory stimulation.[17]

Figure 13 also shows the S/D curves for a cathodal exponential stimulus having the form $I_0\, e^{-t/\tau}$, where I_0 is the peak current and τ is the decay time constant. The exponential current is applicable to capacitive discharge

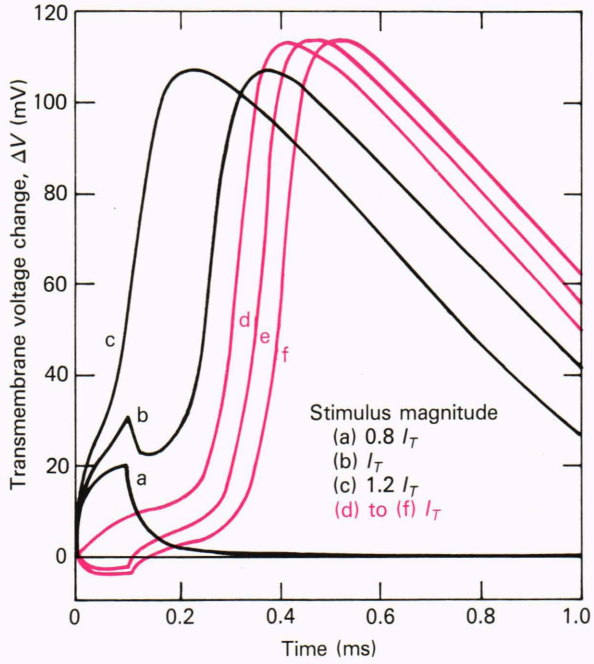

Figure 12—Response of the SENN model to a rectangular monophasic current of 100-μs duration. Curves a-c show the response at the node nearest the electrode for three levels of current. I_T denotes the threshold current. Curves d-f show the propagated response at the next three adjacent nodes for a stimulus at threshold. The example applies to a 20-μm-diameter fiber and a point electrode 2 mm radially distant from the central node (from Reilly et al.[17]).

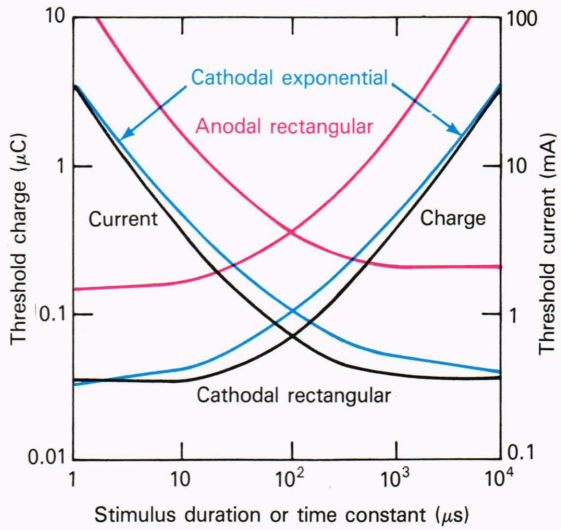

Figure 13—SENN-model strength/duration curves for monophasic stimuli: point electrode stimulation of a 20-μm fiber. The left vertical axis indicates threshold charge for AP initiation. The right vertical axis indicates threshold current. The horizontal axis represents pulse duration for a rectangular stimulus or time constant for an exponential stimulus (from Reilly et al.[17]).

stimuli. These curves are similar to those for a simplified linear model.[18]

As the stimulus duration is reduced, the threshold charge reaches a minimum; for long-duration stimuli, the peak threshold current is minimized. The minimum peak current for a long-duration stimulus is known as the rheobasic current. The exponential and rectangular stimuli have the same minimum charge threshold. At brief durations, sensitivity is not affected by the fine structure of the monophasic pulse waveform.

The shapes of the *S/D* curves in Fig. 13 are similar to the mathematical expressions derived for a linear representation of a membrane,[18]

$$\frac{I_0}{I_{\min}} = \frac{1}{1-e^{-\tau/\tau_m}} \qquad (44)$$

and

$$\frac{Q_0}{Q_{\min}} = \frac{\tau/\tau_m}{1-e^{-\tau/\tau_m}} \ , \qquad (45)$$

where I_0 is the threshold current, Q_0 is the threshold charge given by $I_0\tau$, τ is the duration of a rectangular current pulse, τ_m is the membrane time constant given by the product of membrane resistance (R_m) and capacitance (C_m), $I_{\min}$ is the minimum threshold current for $\tau \to \infty$, and $Q_{\min}$ is the minimum charge for $\tau \to 0$.

In the neural stimulation literature, a measure of the membrane response time is often cited in terms of "chronaxy," which is defined as the threshold duration of a rectangular current pulse whose amplitude is twice the rheobasic current. The relationship of chronaxy to the membrane time constant is readily derived from Eq. 44 by setting $I_0/I_{\min}$ equal to 2 and solving for τ_m. The result is

$$\text{chronaxy} = 0.693\ \tau_m \ . \qquad (46)$$

The shape of the *S/D* curve for a linear *RC* network model of a single node is characterized in Eqs. 44 and 45 by the membrane's exponential time constant, given by the product $R_m C_m$. The SENN model also has a response time that depends on both linear and nonlinear membrane properties and internodal resistance, R_a. Consequently, no single linear circuit parameter specifies the curves in Fig. 13. It is therefore useful to define an equivalent *S/D* time constant (τ_e) in terms of the shape of the *S/D* curve. Here, τ_e is defined as the *RC* time constant of the linear single-node model having an *S/D* curve shape that best matches the shape of a given empirical curve. By using a linear least-squares fit of Eq. 44 to the rectangular current threshold curve in Fig. 13, a value of τ_e of 92.3 μs is obtained. This value differs from the simple product of membrane capacitance and resistance in the subthreshold region of linear response, for which the product $R_m C_m$ is only 66 μs.

The *S/D* time constant is defined here in terms of a best-fitting ideal curve taken from a linear circuit model. The time constant can also be determined by the ratio $Q_{\min}/I_{\min}$.[19] By applying this calculation to the data

displayed in Fig. 13, the S/D time constant is found to be 92 μs. Agreement between this definition and the least-squares fit method is expected if the S/D relation follows the form given by the linear circuit model (Eqs. 44 and 45).

Experimental values of τ_e can be inferred from the S/D curve shape, from chronaxy using Eq. 46, or from Q_{min}/I_{min}. Table 5 presents a summary of τ_e values determined from a variety of experiments. The value of τ_e for the SENN model (about 100 μs) falls within the reported experimental range and is quite close to experimental values reported for in-vivo stimulation. However, many of the experimental time constants for cutaneous stimulation exceed that of the SENN model by a factor of 2 or more. It has been hypothesized[26] that the values of P and τ_e observed with electrocutaneous stimulation may arise from stimulation at neural end structures (e.g., receptors, free nerve endings, and motor neuron end plates).

Current Density and Electric Field Relationships

The thresholds plotted in Fig. 13 were derived for stimulation via a small point electrode near the axon where the spatial distribution of the voltages along the axon follows Eq. 41. To determine the general spatial distribution requirements for neural excitation, we recall that the membrane is depolarized near the cathode and that adequate depolarization ($\approx$ 15 mV) will initiate an action potential. Figure 14 illustrates two bipolar electrode arrangements for stimulating a nerve fiber. In arrangement a, current flow toward the cathode results in membrane depolarization in that region; current flow near the cathode results in hyperpolarization. In arrangement b, the membrane will be hyperpolarized on the side of the axon near the anode and depolarized on the side near the cathode. Various experimental studies have shown that the neuron is relatively insensitive to transverse field stimulation (as in Fig. 14b), relative to longitudinal stimulation (as in Fig. 14a).[27] Such experimental findings correspond with theoretical expectations.[16,28]

In addition to a longitudinal orientation, the electric field must also have a spatial gradient to support excitation. This property can be appreciated by referring to Eq. 39, which shows that second differences of the external voltages drive changes in the membrane potential. If the electric field were uniform and the axon were infinite in both directions, there would in theory be zero net current transfer at every node. However, the field within this biological medium is never uniform. Furthermore, an effective field gradient will be realized if the orientation of the axon changes with respect to a locally uniform field or if the axon is terminated in the field (as with receptors, free nerve endings, or the nerve connections at the muscle fibers).

Uniform field excitation was studied with the SENN model with a 21-node array; the first seven nodes used the nonlinear FH equations. In each case examined, excitation was initiated at the terminal node nearest the cathode, and the threshold was independent of the initial reference voltage, $V_{e,1}$. We interpret this arrangement as representing stimulation at neural end structures.

Table 5—S/D time constants determined from published literature.

τ_e (μs)	*Type of Measurement*	*Comment*	*Ref.*
150	Electrocutaneous sensory	–	20
200	Electrocutaneous sensory	–	21
300	Electrocutaneous sensory	–	22
220	Electrocutaneous sensory	Small electrodes	23
2000	Electrocutaneous sensory	Large electrodes	23
200–900	Electrocutaneous sensory	–	24
20–700	Electromyography	Enervated muscle	25
≥4300	Electromyography	Denervated muscle	25
29	In-vitro mammal nerve	A_β fibers	11
450	In-vitro mammal nerve	A_δ fibers	11
80–100	In-vivo mammal nerve	3- to 13-μm fibers	17

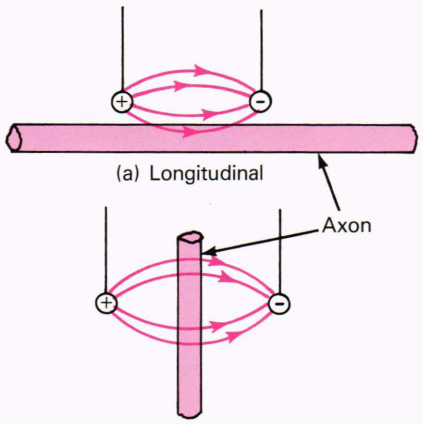

Figure 14—Longitudinal and transverse current excitation.

The threshold curves for uniform field stimulation are similar to the point electrode stimulation curves in Fig. 13, except that the units on the vertical axes must be interpreted differently. Instead of stimulus current, thresholds are expressed in terms of the normalized electric field within the biological medium; instead of threshold charge, thresholds are expressed in terms of the product of field and pulse duration. Alternatively, the uniform field stimulation threshold values can be expressed in terms of current density (J) or charge density (q) by multiplying the previously mentioned values by the conductivity of the

Table 6—Minimum stimulus thresholds with uniform field excitation: single monophasic stimuli.

Criteria		*Fiber Diameter* (μm) *5*	*10*	*20*
A. Field strength criteria				
1. E_{min}	(V/m)	24.6	12.3	6.2
2. $(E\tau)_{min}$	(V·s/m)	2.98×10^{-3}	1.49×10^{-3}	0.75×10^{-3}
B. Current density criteria				
1. J_{min}	(A/m^2)	4.92	2.46	1.23
2. q_{min}	(C/m^2)	6.0×10^{-4}	3.0×10^{-4}	1.5×10^{-4}

Notes: Thresholds A.1 and B.1 apply to long pulses ($\tau \geq 1$ ms). Thresholds A.2 and B.2 apply to short pulses ($\tau \leq 5$ μs). Current and charge density were determined for conductivity $\sigma = 0.2$ S/m.

medium. A linear least-squares fit of the uniform field excitation thresholds to Eq. 44 yields an S/D time constant of $\tau_e = 120$ μs.

Table 6 presents the minimum threshold values (analogous to Q_{min} and I_{min}) used as normalizing factors for the uniform field S/D curves. For long pulses ($\tau \geq 1$ ms), the minimum threshold is expressed in Part A of Table 6 in terms of the induced field. For short pulses ($\tau \leq 5$ μs), the minimum threshold is given in terms of the product of field strength and pulse duration.

The longitudinal separation of nodes in a myelinated fiber is directly proportional to fiber diameter. Therefore, the absolute threshold in a uniform field is inversely proportional to fiber diameter. This relationship can be seen by referring to Eq. 39: if the nodal separation is increased, the external nodal potential differences within a uniform electric field will increase proportionately. Table 6 expresses thresholds for fiber diameters of 5, 10, and 20 μm. These values effectively cover the diameter spectrum of myelinated fibers.

The electric field in the medium is the primary force governing stimulation. However, current density is perhaps a more frequently cited stimulation parameter. Table 6 also expresses thresholds in units of current and charge density. These quantities are determined by multiplying E and $E\tau$ by the conductivity of the medium, σ. In Table 6, the quantities in Part B were obtained from those in Part A by assuming a conductivity of $\sigma = 0.2$ S/m for the bulk conductivity of muscle tissue. The current density and electric field thresholds listed in Table 6 bracket experimentally determined values[29-33] if appropriate allowances are made for waveform and geometric factors.

Excitability Properties with Biphasic Stimuli

The current reversal of a biphasic pulse can reverse a developing AP that was excited by the initial phase. As a result, a biphasic pulse may have a higher threshold than a monophasic pulse. Figure 15 shows S/D curves from the SENN model for three types of stimuli: a monophasic constant-current (rectangular) stimulus, a symmetric biphasic rectangular stimulus, and a sinusoidal stimulus. The data apply to stimulation via a point

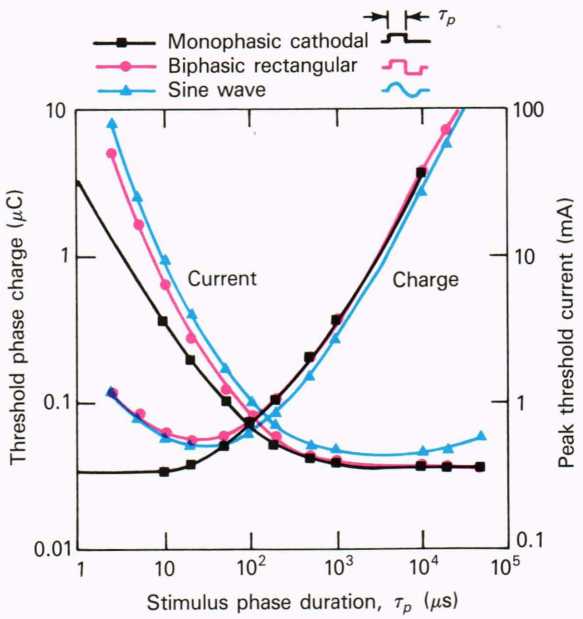

Figure 15—S/D relationships derived from the SENN model: point electrode stimulation of a 20-μm fiber. Current thresholds and charge thresholds are for single-pulse monophasic and for single-cycle biphasic stimuli with initial cathodal phases. Threshold current refers to the peak of the stimulus waveform. Charge refers to a single phase for biphasic stimuli (from Reilly et al.[17]).

electrode 2 mm radially distant from a 20-μm-diameter fiber. The biphasic stimuli consist of a single stimulus cycle with an initial cathodal phase followed by an anodal phase of the same duration and equal magnitude. The phase duration indicated by the horizontal axis is that for the initial cathodal half-cycle. Stimulus magnitude is given in terms of peak current on the right vertical axis and in terms of the charge in a single monophasic phase of the stimulus on the left vertical axis. The charge is computed from $Q = I\tau$ for the rectangular waveforms and is given by $Q = (2/\pi)I\tau$ for the sinusoidal waveforms, where I is threshold current amplitude and τ is phase duration.

The effect of current reversal in the biphasic waveforms is to increase the threshold requirement for a propagating AP. This situation can be seen in Fig. 15 by comparing the monophasic and biphasic rectangular stimulus thresholds. For long durations, the threshold current is the same for the two stimuli. However, as the stimulus duration becomes short relative to the equivalent S/D time constant (about 100 μs), the biphasic current has an elevated threshold. The degree of elevation is magnified as the stimulus duration is reduced.

The thresholds illustrated in Fig. 15 apply to stimuli with an initial cathodal phase. Thresholds are greater if the initial phase is anodal, but only if the phase duration is less than 100 μs. For a single cycle of a sine wave, the SENN model shows that if the initial phase of the stimulus is anodal, thresholds are greater than initial cathodal thresholds by 5% at a phase duration of 100 μs, 10% at 50 μs, 45% at 10 μs, and 60% at 5 μs.

Figure 16 illustrates threshold multipliers (M) based on the SENN model for biphasic rectangular pulses with uniform field excitation. The vertical axis gives the threshold multiplier for a double pulse relative to a single pulse. The portion of Fig. 16 above $M = 1$ applies to a biphasic pulse doublet, where the current reversal has the same magnitude and duration as the initial pulse. The portion of Fig. 16 below $M = 1$ is for a monophasic pulse doublet. Figure 16 applies if the initial pulse is cathodal. Stimulation is also possible with an initial anodal pulse, but the thresholds are elevated.

According to Fig. 16, biphasic threshold elevation depends on the pulse duration and the time delay before current reversal. Thresholds are most elevated when the pulse is short and the current reversal immediately follows the initial pulse. If the phase reversal is delayed by 100 μs or more, there is little detectable effect on the threshold. An implication of the results shown in Figs. 15 and 16 is that the membrane integrates the stimulus over a duration roughly equal to the equivalent S/D membrane time constant. This integration is nonlinear: the biphasic waveforms all inject zero net charge but have finite threshold magnitudes.

There are relatively few experimental data for biphasic stimuli with which to compare SENN model results. One study tested sensory sensitivity to biphasic pulses having phase durations of 20 to 50 μs, with delays from 10 to 50 μs.[34] The reported ratios among thresholds were within a few percent of the multiplier obtained with the SENN model (Fig. 16). Another study using damped cosine waves demonstrated that the phase reversal of an oscillating stimulus can elevate thresholds relative to a monophasic stimulus.[35]

The biphasic threshold data of Fig. 15 can be represented by strength/frequency (S/F) curves, as shown in Fig. 17. The horizontal axis in Fig. 17 is the inverse of twice the phase duration in Fig. 15. Figure 17 also shows the threshold curve for continuous sinusoidal stimulation.[17]

Figure 17 includes experimental threshold curves for human perception and muscle contraction.[36,37] The experimental curves have been arbitrarily scaled on the vertical axis to facilitate comparison of the curve shapes. The shapes of the experimental and continuous stimulation SENN curves correspond reasonably well, considering that continuous stimulation was used in the cited experimental studies. The high-frequency upturn is also consistent with other sensory data[38] and is due to the biphasic membrane integration effects discussed earlier. Below 40 Hz, thresholds rise for sinusoidal stimulation. At low frequencies, the slow rate of change of the sinusoid prevents the membrane from building up a depolarizing voltage because membrane depolarization is counteracted by membrane leakage. In contrast, square-wave

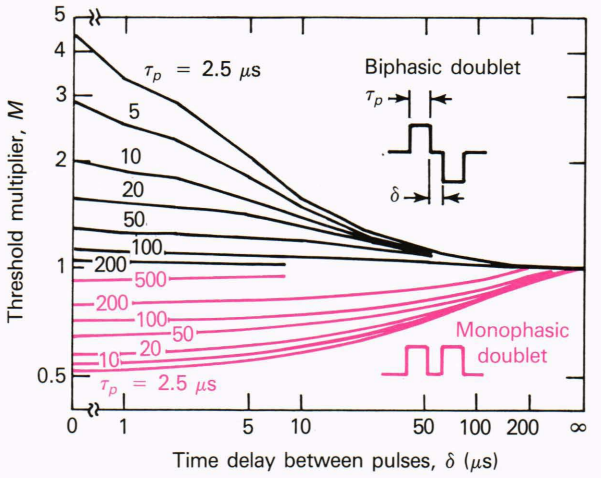

Figure 16—Threshold multipliers for biphasic and monophasic pulse doublets. Uniform field excitation of truncated axon.

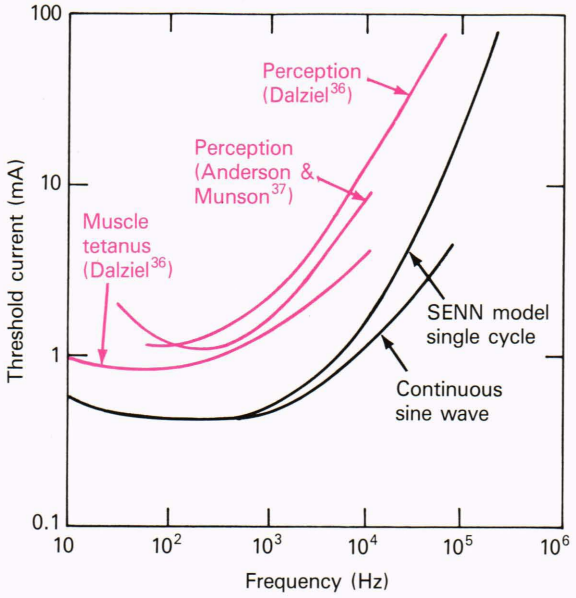

Figure 17—S/F curves for sinusoidal current stimuli. Upper curves are from experimental data.[36,37] Lower curves apply to the SENN model. Experimental curves have been shifted vertically to facilitate comparisons (adapted from Reilly et al.[17]).

biphasic stimuli do not have a rate of change that depends on frequency. Consequently, no upturn in thresholds occurs at low square-wave frequencies.

Repetitive Stimuli

Repetitive stimuli can be more potent than a single stimulus through threshold reduction or through response enhancement because of multiple AP generation. In both cases, an integration effect of the multiple pulses occurs. In the first case, the integration takes place at the membrane level. In the second, response enhancement takes place at higher levels within the central nervous system for neurosensory effects and at the muscle level for neuromuscular effects.

The lower section of Fig. 16 illustrates multiple pulse threshold effects for two pulses of the same polarity. The figure gives the threshold multiplier relative to that for a single pulse when there are two pulses of stimulation. The effects are most pronounced for short pulses and short interpulse delays. (In this representation, a delay of zero is really the same as a single pulse of twice the duration.) Even at a delay of 200 μs, the integrative effects of a second pulse reduce the threshold by about 10% for $\tau_p \leq 20$ μs. The SENN model was also exercised to evaluate the threshold modification for sequences of pulses, N_p, numbering 1, 2, 4, 8, 16, 32, 64, and 128. Figure 18 illustrates the results for $\tau_p = 10$, 50, and 100 μs and for $\delta = 10$, 50, 100, 200, and 500 μs. As in Fig. 16, the vertical axis gives the threshold multiplier relative to a single pulse. The curve labeled $\delta = 0$ applies to continuous stimulation. Threshold reduction due to pulse integration is increased as the pulse duration and delay time are shortened. At a delay of 500 μs, the SENN model shows no measurable pulse integration effect.

Bütikoffer and Lawrence[39] used the FH equations at a single node to quantify the integrative effects of multiple pulses having a duration of 50 μs and a delay of 250 μs. The threshold for five pulses was reduced about 20% relative to a single pulse, and most of that reduction was achieved by the third pulse. Even for pulse delays as long as 5 ms, cutaneous perception threshold reductions on the order of 7 to 8% have been reported for continuous pulse trains with pulse durations from 100 to 400 μs.[22]

SUMMARY AND DISCUSSION

A principal motivation for this work was to provide a predictive framework for assessing the excitatory potency of electric currents. The SENN model discussed here incorporates spatial and temporal aspects of the stimulus current into a theoretical model that accounts for a variety of experimental relationships.

For simple monophasic currents applied locally, the relevant parameters governing stimulus potency depend on the time scale of the stimulus. For stimuli that are short relative to the depolarization processes of the membrane, the relevant parameter is the stimulus charge. Within this brief time interval, the details of the stimulus waveform are practically unimportant. On the other hand, if the duration of a monophasic stimulus is long compared with the depolarization time, the relevant parameter is peak stimulus current. At neither extreme is stimulus energy a relevant parameter, as has been commonly supposed.

Excitation by biphasic stimuli is more complex because the current reversal may be able to reverse the excitatory process that is started by the initial phase. In that case, the details of the current waveshape and its temporal scale relative to the depolarization time constant are crit-

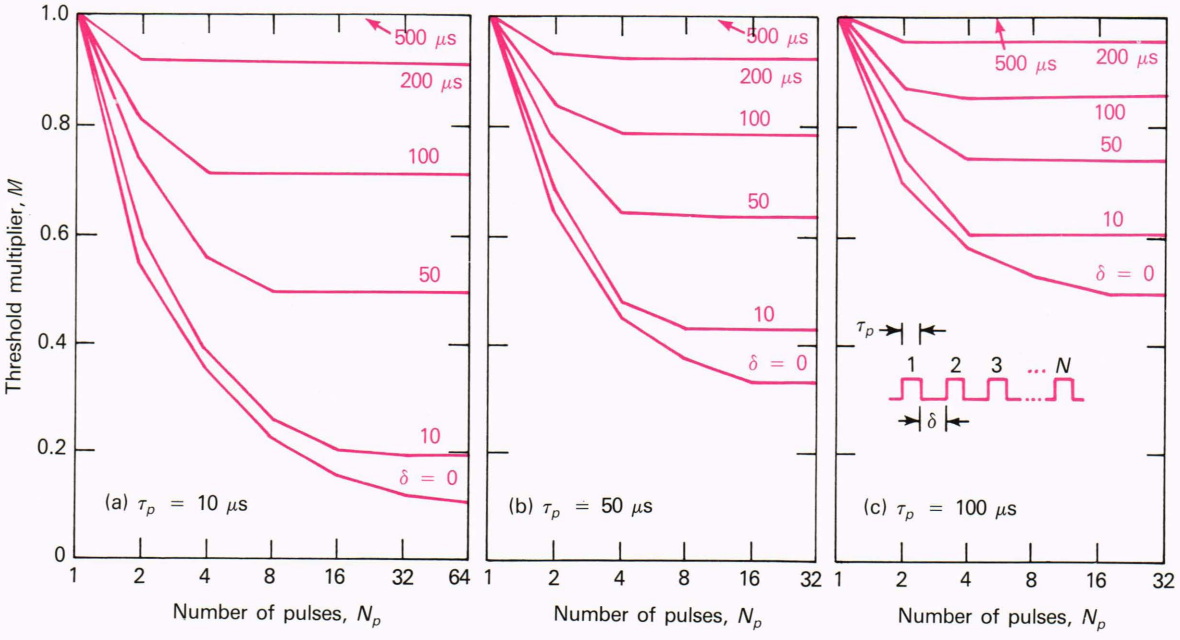

Figure 18—Threshold multipliers for repetitive pulse sequences – thresholds evaluated at $N_p = 1, 2, 4, 8, 16, 32$, and 64. Uniform field excitation of truncated axon.

ical factors. If the current reversal is accomplished on a short time scale, excitation thresholds are elevated. On the other hand, if the biphasic wave is repeated, thresholds can be reduced to a level below that for a single monophasic pulse.

The SENN model described here is able to represent a broad range of stimulus relationships. As such, it represents a useful tool for understanding experimental data and for predicting effects that are not readily studied experimentally.

REFERENCES

[1] J. P. Reilly and W. D. Larkin, "Understanding Electric Shock," *Johns Hopkins APL Tech. Dig.* **5**, 296–304 (1984).

[2] T. C. Ruch and H. D. Patton, eds., *Physiology and Biophysics*, W. B. Saunders, Philadelphia, pp. 157–200 (1979).

[3] B. Katz, *Nerve Muscle and Synapse*, McGraw-Hill, New York (1966).

[4] A. L. Hodgkin and A. F. Huxley, "A Quantitative Description of Membrane Current and Its Application to Conduction and Excitation in Nerve," *J. Physiol.* **117**, 500–544 (1952).

[5] B. Frankenhaeuser and A. F. Huxley, "The Action Potential in the Myelinated Nerve Fiber of *Xenopus Laevis* as Computed on the Basis of Voltage Clamp Data," *J. Physiol.* **171**, 302–315 (1964).

[6] R. B. Stein, *Nerve and Muscle*, Plenum Press, New York (1980).

[7] H. Motz and F. Rattay, "A Study of the Application of the Hodgkin–Huxley and the Frankenhaeuser–Huxley Model for Electrostimulation of the Acoustic Nerve," *Neurosci.* **18**, 699–712 (1986).

[8] M. A. Brazier, *Electrical Activity of the Nervous System*, Williams & Williams, Baltimore (1977).

[9] A. S. Paintal, "A Comparison of the Impulses of Mammalian Non-Medulated Nerve Fibers with Those of the Smallest Diameter Medulated Fibers," *J. Physiol.* **193**, 523–538 (1967).

[10] A. S. Paintal, "Conduction in Mammalian Nerve Fibers," in *New Developments in Electromyography and Clinical Neurophysiology*, J. E. Desmedt, ed., Karger, Basel, Switzerland, Vol. 2, pp. 19–41 (1973).

[11] C. L. Li and A. Bak, "Excitability Characteristics of the A- and C-Fibers in a Peripheral Nerve," *Exp. Neurol.* **50**, 67–79 (1976).

[12] E. R. Kandel and J. B. Schwartz, *Principles of Neural Science*, Elsevier/North Holland, New York (1981).

[13] J. W. Cooley and F. A. Dodge, "Digital Computer Solutions for Excitation and Propagation of the Nerve Impulse," *Biophys. J.* **6**, 583–599 (1966).

[14] R. FitzHugh, "Computation of Impulse Initiation and Saltatory Conduction in a Myelinated Nerve Fiber," *Biophys. J.* **2**, 11–21 (1962).

[15] H. Bostock, "The Strength–Duration Relationship for Excitation of Myelinated Nerve: Computed Dependence on Membrane Parameters," *J. Physiol.* **341**, 59–74 (1983).

[16] D. R. McNeal, "Analysis of a Model for Excitation of Myelinated Nerve," *IEEE Trans. Biomed. Eng.* **BME-23**, 329–337 (1976).

[17] J. P. Reilly, V. T. Freeman, and W. D. Larkin, "Sensory Effects of Transient Electrical Stimulation—Evaluation with a Neuroelectric Model," *IEEE Trans. Biomed. Eng.* **BME-32**, 1001–1011 (1985).

[18] J. P. Reilly and W. D. Larkin, "Electrocutaneous Stimulation with High Voltage Capacitive Discharges," *IEEE Trans. Biomed. Eng.* **BME-30**, 631–641 (1983).

[19] D. Noble and R. B. Stein, "The Threshold Conditions for Initiation of Action Potentials by Excitable Cells," *J. Physiol.* **187**, 129–162 (1966).

[20] J. P. Girvin, L. E. Marks, J. L. Quest, D. O. O'Keefe, P. Ning, and W. H. Dabelle, "Electrocutaneous Stimulation – I. The Effects of Stimulus Parameters on Absolute Threshold," *Percept. Psychophys.* **32**, 524–528 (1982).

[21] G. B. Rollman, "Electrocutaneous Stimulation," in *Conference on Cutaneous Communication Systems and Devices*, F. A. Geldard, ed., The Psychonomic Society, Austin, Tex., pp. 38–51 (1974).

[22] J. F. Hahn, "Cutaneous Vibratory Thresholds for Square-Wave Electrical Pulses," *Science* **127**, 879–880 (1958).

[23] E. A. Pfeiffer, "Electrical Stimulation of Sensory Nerves with Skin Electrodes for Research, Diagnosis, Communication, and Behavioral Conditioning: A Survey," *Med. Biol. Eng.* **6**, 637–651 (1968).

[24] W. D. Larkin and J. P. Reilly, "Strength/Duration Relationships for Electrocutaneous Sensitivity: Stimulation by Capacitive Discharges," *Percept. Psychophys.* **36**, 68–78 (1984).

[25] Y. T. Oester and S. H. Licht, "Routine Electrodiagnosis," in *Electrodiagnosis and Electromyography*, S. H. Licht, ed., E. Licht, New Haven, Conn., pp. 201–217 (1971).

[26] J. P. Reilly and R. H. Bauer, "Application of a Neuroelectric Model to Electrocutaneous Sensory Sensitivity: Parameter Variation Study," *IEEE Trans. Biomed. Eng.* **BME-34**, 752–754 (1987).

[27] J. B. Ranck, "Which Elements are Excited in Electrical Stimulation of Mammalian Central Nervous System: A Review," *Brain Res.* **98**, 417–440 (1975).

[28] D. R. McNeal and D. A. Teicher, "Effect of Electrode Placement on Threshold and Initial Site of Excitation of a Myelinated Nerve Fiber," in *Functional Electrical Stimulation*, T. F. Hambrecht and J. B. Reswick, eds., Marcel Dekker, New York (1977).

[29] D. McRobbie and M. A. Foster, "Thresholds for Biological Effects of Time-Varying Magnetic Fields," *Clin. Phys. Physiol. Meas.* **5**, 67–78 (1984).

[30] M. J. R. Polson, A. T. Barker, and S. Gardiner, "The Effect of Rapid Rise-Time Magnetic Fields on the EEG of the Rat," *Clin. Phys. Physiol. Meas.* **3**, 231–234 (1982).

[31] M. J. R. Polson, A. T. Barker, and I. L. Freeston, "Stimulation of Nerve Trunks with Time-Varying Magnetic Fields," *Med. Biol. Eng. Comput.* **20**, 243–244 (1982).

[32] S. Ueno, K. Harada, C. Ji, and Y. Oomura, "Magnetic Nerve Stimulation Without Interlinkage Between Nerve and Magnetic Flux," *IEEE Trans. Magn.* **MAG-20**, 1660–1662 (1984).

[33] D. D. Irwin, S. Rush, R. Evering, E. Lepeschkin, D. B. Montgomery, and R. J. Weggel, "Stimulation of Cardiac Muscle by a Time-Varying Magnetic Field," *IEEE Trans. Magn.* **MAG-6**, 321–322 (1970).

[34] R. Bütikoffer and P. D. Lawrence, "Electrocutaneous Nerve Stimulation-II: Model and Experiment," *IEEE Trans. Biomed. Eng.* **BME-25**, 526–531 (1979).

[35] J. P. Reilly and W. D. Larkin, "Mechanisms for Human Sensitivity to Transient Electric Currents," in *Electrical Shock Safety Criteria*, J. E. Bridges, G. L. Ford, I. A. Sherman, and M. Vainberg, eds., Pergamon Press, New York, pp. 241–249 (1985).

[36] C. F. Dalziel, "Electric Shock Hazard," *IEEE Spectrum* **9**, 41–50 (1972).

[37] A. B. Anderson and W. A. Munson, "Electrical Stimulation of Nerves in the Skin at Audio Frequencies," *J. Acoust. Soc. Am.* **23**, 155–159 (1951).

[38] I. Chatterjee, D. Wu, and O. P. Gandhi, "Human Body Impedance and Threshold Currents for Perception and Pain for Contact Hazard Analysis in the VLF-MF Band," *IEEE Trans. Biomed. Eng.* **BME-33**, 486–494 (1986).

[39] R. Bütikoffer and P. D. Lawrence, "Electrocutaneous Nerve Stimulation – II: Stimulus Waveform Selection," *IEEE Trans. Biomed. Eng.* **BME-26**, 69–75 (1979).

THE AUTHOR

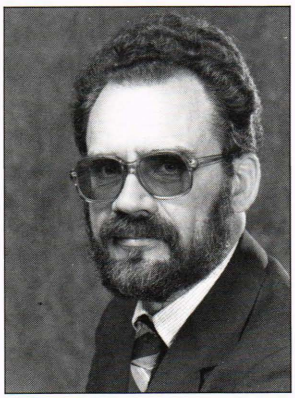

J. PATRICK REILLY received the B.E.E. degree from the University of Detroit in 1962 and the M.S.E. degree from The George Washington University in 1976. He is a member of APL's Principal Professional Staff. After joining APL in 1962, he worked on a variety of theoretical and experimental projects associated with radar and sonar systems, with emphasis on signal processing, system studies, and reflections from targets and the natural environment. Mr. Reilly later supervised the Electromagnetics and Acoustics Section of the Environmental Assessment Group, where he was responsible for studies of electromagnetic and acoustic interactions with environmental and biological systems. In this connection, he was director of a research program on human reactions to transient electric currents. He is now with APL's Fleet Systems Department, where he is responsible for radar systems studies and for bioelectric research activities. He is a senior member of the IEEE and a member of the Bioelectromagnetics Society.